4. Study of tribological properties of multilayer Ti/TiN coating containing stress absorbing layers.

**Work published in ASME Journal of Tribology [215]*

Titanium (Ti)/Titanium Nitride (TiN) ultrathin multilayer coating was deposited on 100Cr6 substrates to investigate the friction and wear behavior in the presence of paraffin oil as a lubricant. The coating architecture was designed by adding thick stress absorbing layers (SAL ~320 nm) in between the ultrathin Ti/TiN (3.5/4 nm) multilayer structure. The SAL reduces the residual stress in the coating. The coating had a NaCl type of structure, and XRD results showed the preferential crystallographic orientation of TiN along [111] direction. The tribological properties of the nanostructured coating were evaluated under reciprocating sliding conditions at varying load (2 and 7N), and temperature (30 and 100 °C) against 100Cr6 steel balls using paraffin oil as a lubricant. There was no considerable change in the CoF at different testing parameters. However, there was a significant drop in wear volume at high-temperature testing conditions. The worn tracks were analyzed for their morphology and elemental composition through SEM, EDAX, and Raman spectroscopy.

4.1. Introduction.

Tribological problems due to friction and wear are one of the major concerns of the industries. The cutting tools, automobile, and aircraft industries require solution related to these tribological problems. The multifunctional thin film physical vapour deposition (PVD) coatings have been used in industries widely to provide unique solutions to the problems arising from friction and wear [86,216,217]. These coatings have superior mechanical, chemical, and high-temperature properties. Today, we can design novel coatings in the form of nanocomposite and multilayer arrangements, which are tailored to meet the desirable properties

[31,96,133,134,218–220]. Over the past few decades, a significant amount of work has been done on the binary transition metal nitride coatings such as titanium nitride (TiN), chromium nitride (CrN), and tungsten nitride (WN), etc. [22,221,222]. Among these transition metal nitride coatings, TiN coatings have been reported in many studies because of their high wear resistance, corrosion resistance, chemical stability, and high-temperature properties. The tribological properties of these hard and brittle TiN coatings are very much affected by the residual compressive stresses. It leads to a fracture in the coating (cohesive failure) and delamination of the coating from the substrate (adhesive failure), which in turn limits the thickness of the coating.

Therefore, the objective is to obtain a coating of higher thickness and hardness without increasing the brittleness and residual stresses in the coating. Many researchers have reported that the coatings comprising of hard/soft layers improve the tribological properties than a single-layered hard coating [223–226]. Lackner et al. [114] reported that the fracture resistance of the hard coating could be increased by diminishing the bending stress in the coating. The introduction of a single soft layer drastically decreases the bending stress by reducing the thickness of a single hard layer and acting as shear zones on which hard layer can slide relative to the other layers below. The TiN coatings generally consist of compressive residual stresses, therefore introducing soft and ductile titanium (Ti) layer controls the residual stress levels and improves the adhesion of the coating [227].

In the earlier investigation, multilayer Ti/TiN coating was optimized for higher toughness [228]. The bilayer thickness of the films was ranged from 7.5 – 112 nm and the film with bilayer thickness of 7.5 nm showed better resistance to crack propagation than the other films. Although the coating with a bilayer thickness of 7.5 nm showed better resistance to crack propagation, the residual stress was quite high. Therefore, the nanolayered Ti/TiN coating was optimized with stress absorbing layers (SAL) of Ti for the reduced residual stress and high

scratch resistance [229]. In this work, the tribological behavior of this coating having least residual stress has been studied in the lubricated environment at 30 and 100 °C, respectively. Paraffin oil was used as a lubricant, as it is the most used and studied lubricant for industrial applications. Also, paraffin oil is widely used as base stock in lubricants and greases [213,230,231] . Moreover, hard coatings of CrN and TiN are widely being explored for application on piston rings [232]. Therefore, it is imperative to study the tribological properties of this novel ultrathin multilayer Ti/TiN coating in presence of paraffin oil. As mentioned above, many researchers have published the tribological studies of TiN coatings, and very few of them discusses the role of titanium dioxide (TiO_2) formed in situ during tribochemical reaction. Nothing is reported about the phases of TiO_2 formed during tribochemical reaction. Also, no literature is available for tribological study of multilayer Ti/TiN coating having bilayer thickness of 7.5 nm, containing thick metal layers in its coating architecture. Different forms of TiN coatings have been widely used to coat cylinder liners in piston cylinder engine to reduce wear and friction [233]. Therefore, it is imperative to study the wear behavior of Ti/TiN multilayer coatings whose architecture has been modified by adding thick Ti SAL. The highest testing temperature was kept at 100 °C, because paraffin oil starts losing its viscosity at higher temperature. The wear scars were analyzed with SEM, EDAX, and Raman spectroscopy, to know the wear mechanism involved during the tribological contact condition.

4.2. Material and methods.

Ti/TiN coating was deposited on 100Cr6 steel (25.4 mm diameter and 8 mm thick) and silicon substrates. Reactive unbalanced magnetron sputtering equipped with four targets was used, and the targets were powered by pulsed DC power sources. All the cathodes equipped with 6-inch titanium targets (99.9 % purity) were used for deposition. The deposition process of this system

has been explained in the section 3.2.1. The substrates were loaded into the vacuum chamber, and the pressure inside the chamber was pumped down to 9 X 10^{-6} mbar. A DC bias of -1000 V was applied to the substrates, and the substrates were sputter etched in argon plasma for 60 min to remove any oxide layers present on the surface. A Ti interlayer was deposited on the substrates for better adhesion of the coatings. The Ti/TiN multilayer was deposited by pulsing nitrogen (N_2) gas into the chamber. The bilayer period of the multilayer coating was 7.5 nm, with nitride and metal layer thickness of 4.5 and 3 nm, respectively. After every stack of 866 multilayers, a metal Ti layer of 320 nm thickness was introduced as SAL. The detailed deposition parameters are listed in Table 4.1.

Table 4.1. Parameters for coating deposition.

Parameters	Values
Ti target power (interlayer deposition)	250 W
Ti target power (coating deposition)	500 W
N_2 flow rate	11 sccm
Ar flow rate	35 sccm
Bias voltage (coating deposition)	-65 V
Substrate temperature	225 °C

The phase distribution and crystal structure of the coating were analyzed by X-ray diffraction with Cu K_α radiation having a grazing angle of 0.5° and 2Θ resolution of 0.01°. The hardness of the coating was measured in nanoindentation hardness tester coupled with a Berkovich diamond indenter, having resolution and force resolution of 0.04 nm and 0.04 µN, respectively. A total of 8 indentations were done, and the maximum load applied was of 5 mN. The hardness and elastic modulus were obtained from the Oliver and Pharr method [214] by analyzing the loading and unloading curve obtained from the nanoindentation testing.

The cross-sectional morphology of the coating was studied using field emission electron microscopy. The Si substrates were cut, and the cross-section of the substrate was molded and polished before treating with the Kroll's solution. The Kroll's solution, etches the Ti layer, and both Ti and TiN layer can be then seen distinctly.

Reciprocating sliding tests were conducted to investigate the tribological properties of the multilayer coating. 10 mm diameter hardened 100Cr6 steel ball was used to slide against the coated substrates under lubricated and non-lubricated conditions. The normal load applied was 2 and 7N corresponding to 0.5 and 1 GPa of Hertzian contact stress, respectively. Sliding frequency of 5 Hz and a stroke of 1 mm was given to the reciprocating table. The tests were conducted at 30 and 100 °C for 18000 cycles. **Figure 3.5.** shows the schematic diagram of the test setup used for tribotesting, and the detailed description of the reciprocating sliding tribometer can be found in the section 3.6.1. CoF was calculated by first determining the frictional energy. The frictional energy is the area under the frictional hysteresis loop (**Figure** 4.1), which corresponds to the frictional energy dissipated in one complete oscillation, i.e., two times of the stroke. After determining the frictional energy, the average frictional force was calculated for the whole cycle, which is defined as the ratio of frictional energy to the total distance travelled by the disc during testing. Finally, the average CoF for the whole cycle was calculated by dividing the average frictional force with the load applied. Wear volume measurements were done by calculating the total volume loss of the ball and disk specimen. The equations (1-6) were used to calculate volume losses.

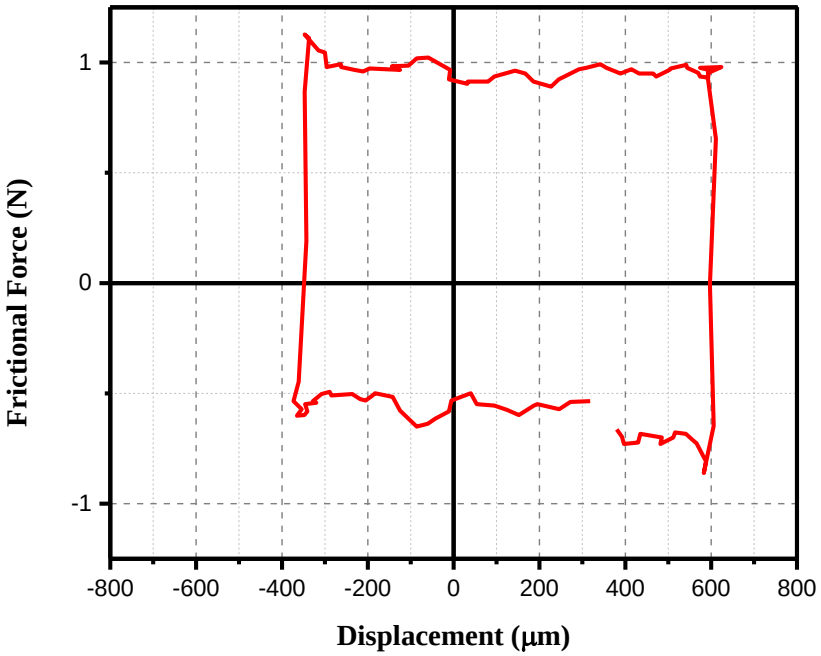

Figure 4.1. A typical hysteresis loop of frictional force and displacement.

$$W_{\text{l,flat}} \approx R' - \sqrt[2]{R'^2 - \frac{{d_\text{p}}^2}{4}} \tag{4.1}$$

$$W_\text{q} \approx \frac{{d_\text{p}}^3}{12R'} \tag{4.2}$$

$$W_{\text{l,ball}} \approx R - \sqrt[2]{R^2 - \frac{{d_\text{p}}^2}{4}} - \; W_{\text{l,flat}} \approx \frac{{d_\text{pa}}^2}{8}\left(\frac{1}{R} - \frac{1}{R'}\right) \tag{4.3}$$

$$W_{\text{v,flat}} \approx \frac{\pi {d_\text{p}}^2 W_{\text{l,flat}}}{8} + \Delta x W_\text{q} \tag{4.4}$$

$$W_{\text{v,ball}} \approx \frac{\pi {d_\text{p}}^2 W_{\text{l,ball}}}{8} \tag{4.5}$$

$$W_\text{v} \approx \; W_{\text{v,flat}} + \; W_{\text{v,ball}} \tag{4.6}$$

Where R' is the approximate radius of curvature of the wear scar on the flat surface after sliding. R' was obtained by curve fitting the profile of the wear scar in the software itself. R is the radius

of the ball. d_p and d_{pa} are the diameter of the wear scar perpendicular and parallel to the direction of sliding, respectively. W_q is the planimetric wear. $W_{l,flat}$ and $W_{l,ball}$ corresponds to linear wear of flat surface and the ball, respectively. Similarly, $W_{v,flat,}$ and $W_{v,ball}$ corresponds to the volumetric wear of flat surface and the ball, respectively. W_v is the total volumetric wear of both ball and the flat surface. The schematic representation of all the notations is also shown in **Figure** 4.2.

The chemical elemental analysis of the worn scars was carried out using SEM appended with energy dispersive X-ray (EDX) spectroscopy and micro- Raman spectroscopy equipped with an argon-ion laser of wavelength 532 nm as an excitation source.

4.3. Results and Discussion.

4.3.1. SEM analysis of the coated surface.

Figure. 4.3 shows the cross-sectional FESEM image of ultrathin multi-layered Ti/TiN coatings. The thick Ti SAL (320 nm), which were introduced to reduce the internal stress and to increase the adhesion of the coating, and it is clearly visible. The bilayer thickness of the coating is 7.5 nm with Ti and TiN layer thickness of 3 and 4.5 nm, respectively. The inset in **Figure** 4.3 shows TiN (bright), and Ti (dark) bands and these are viewed at higher magnification. The total thickness of the film is 9 μm comprising of three stacks of ultrathin Ti/TiN multilayer (866 layers each) and two Ti SAL. It is clear from Fig. 4 that the Ti/TiN multilayer has a columnar structure.

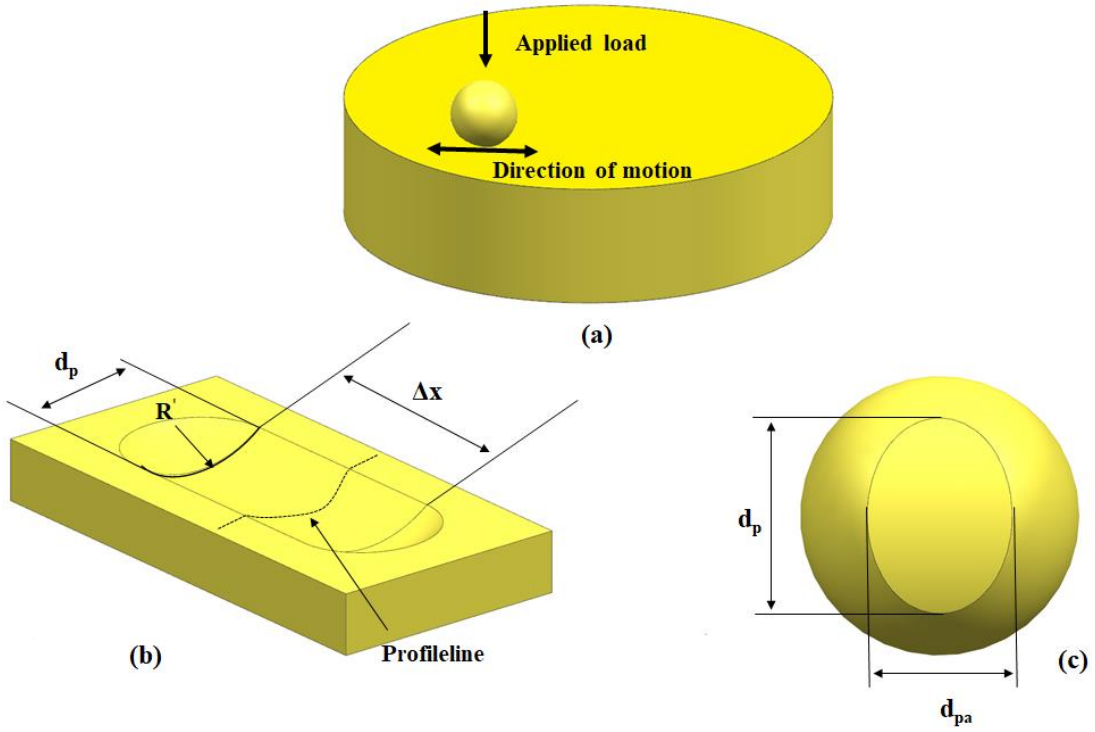

Figure 4.2. Schematic representation of (a) ball on disk arrangement (b) wear scar on flat surface (c) wear scar on the ball.

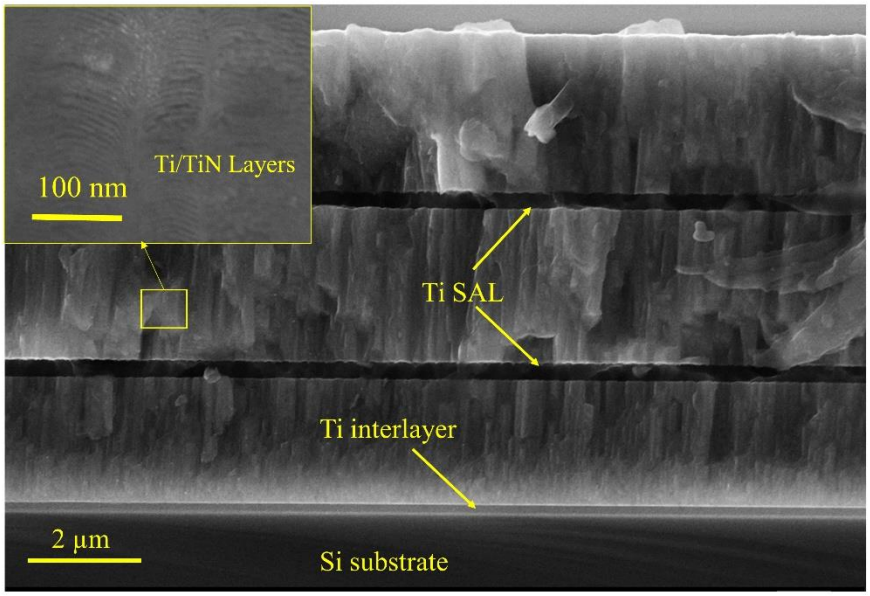

Figure 4.3. The cross-sectional view of ultrathin Ti/TiN coating with SAL. The inset shows the high-resolution image of a Ti/TiN multilayer stack.

4.3.2. XRD analysis of the coating.

Figure 4.4 shows the X-ray diffraction pattern of the Ti/TiN coating. The peaks were deconvoluted using voigt function to indicate the presence of the Ti phase. The diffraction peaks can be assigned to the hexagonal close-packed phase of Ti (JCPDS #44-1294) and face-centered cubic phase of TiN (JCPDS #38-1420). The weak presence of Ti peaks in comparison of TiN peaks is due to diffusion of nitrogen into these layers and presence of residual nitrogen gas in the chamber, which forms non-stoichiometric TiN [228,229]. In one of our investigations, the XRD of Ti/TiN without SAL (Fig. 3(c-d) [228]) and Ti/TiN coating with SAL (in the present work) appear to be similar, which is ascribed to use of low grazing angle (0.5°) during the measurements. At low grazing angles the XRD data is collected only from top layers of the film. The bright-field TEM image is provided in the **Figure** 4.5. shows the presence of thick Ti SAL along with Ti and TiN multilayers as dark and bright lines, respectively. The detailed TEM and selected area electron diffraction analysis is reported in our previous investigation [229], which gives a clear picture of the N diffusion. In which the Ti/TiN multilayer structure had the face-centered cubic phase while the SAL region had the hexagonal closed -packed phase. The TEM image shows many dark spots in Ti/TiN multilayer region; these dark spots are the sites of lattice strains. The face-centered cubic phase of Ti and TiN has almost similar lattice constants. Hence, coherency strain occurs during the epitaxial growth within a columnar nano-crystal [229].

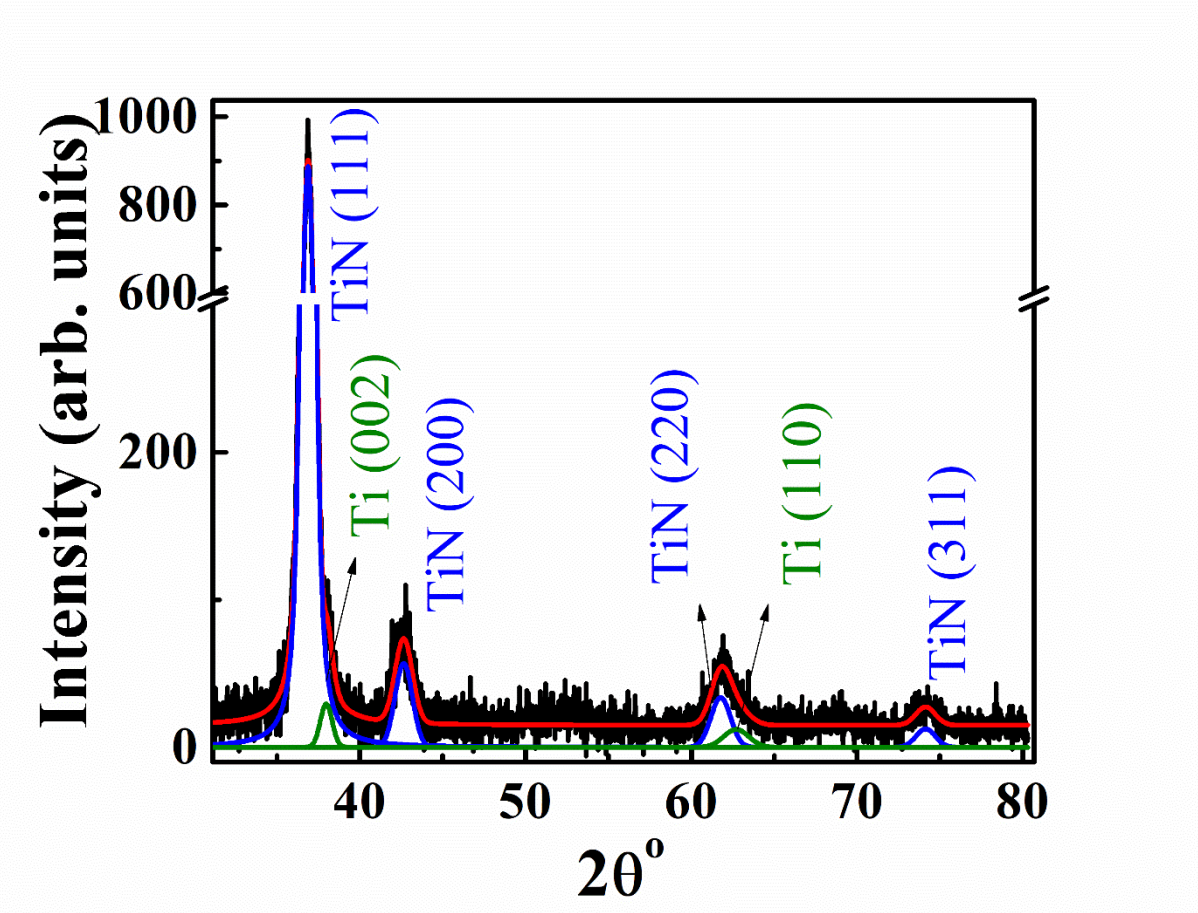

Figure 4.4. XRD pattern of ultrathin multilayer Ti/TiN coating with SAL.

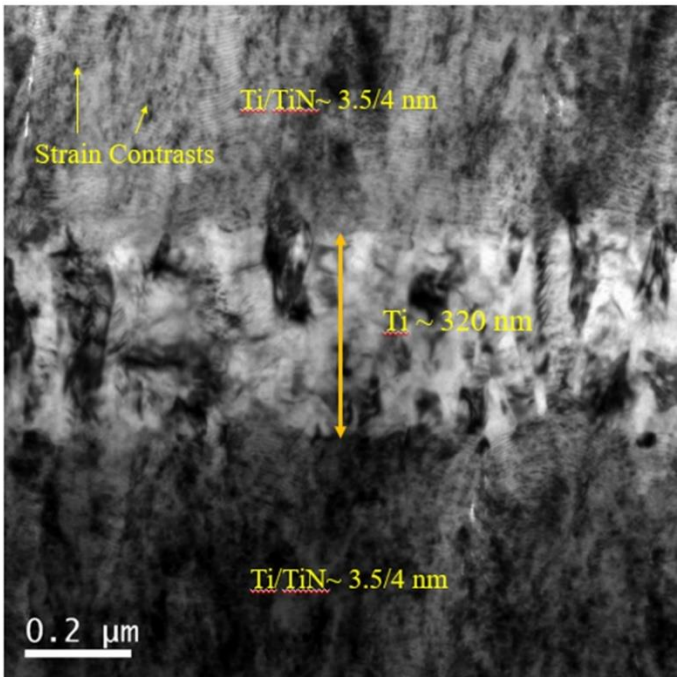

Figure 4.5. TEM image of cross-section of Ti/TiN multilayer coatings.

4.3.3. Tribological performance of the coating

4.3.3.1. Friction behaviour of the coated surface with lubrication

The tribological performance of the coated surface was determined in the presence of paraffin oil. **Figure** 4.6 shows the variation of the coefficient of friction at different loads and temperatures for lubricated and unlubricated conditions. The average coefficient of friction was slightly higher when tested at 100 °C than the one tested at 30 °C. This can be attributed to the loss of viscosity of the paraffin oil at higher temperatures. The minimum film thickness was calculated with the help of Hamrock and Dowson equation [234], considering the elastohydrodynamic lubrication contacts for viscous-elastic regime. The equation is given as:

$$\frac{h_{min}}{R'} = 3.63\left(\frac{u\eta_0}{E'R'}\right)^{0.68}(\xi E')^{0.49}\left(\frac{w}{E'R'^2}\right)^{-0.073}(1 - e^{-0.68k}) \quad (7)$$

Where h_{min} is the minimum film thickness, R' is the reduced radius of curvature, u being the mean velocity, $\eta_0$represents the dynamic viscosity of the lubricant, E' being the reduced elastic modulus, ξ is the pressure velocity coefficient, w is the applied load, and k is the elliptical parameter. The h_{min} calculated from equation 7 for 2 and 7 N load was 4.15 and 3.78 nm, respectively. According to the theory of fluid film lubrication, Hamrock et.al. [235] states that if the value of lambda ratio ($\lambda = \frac{h_{min}}{\sigma^*}$,) is less than 1, then it is under boundary lubrication. The σ^* is the composite surface roughness i.e. $\sigma^* = \sqrt{\sigma_1^2 + \sigma_2^2}$, where $\sigma_1$and σ_2 are the surface roughness of the two mating bodies. The lambda ratio for 2 and 7 N load was found to be 0.05 and 0.06, respectively. Which indicates that the sliding contacts were in boundary lubrication regime. Further, during tribotesting, only a small drop of oil was used, and the CoF values (> 0.1) from **Figure** 4.6 also indicate that the lubrication regime is in boundary regime. Therefore, the friction not only depends on the interactions of the contact surfaces but also on the interaction between the contact surfaces and the lubricant. A higher viscosity fluid can maintain

a higher film thickness, and the contact with surface asperities is reduced, and the wear debris decreases, which in turn leads to a lower coefficient of friction [236]. However, the average coefficient of friction at 7N load is about 10% lower as compared to 2N load at both the temperatures. A similar kind of behaviour was also observed when the coating was tested in unlubricated condition (**Figure** 4.6). This small difference can occur due to deformation of surface asperities at higher load. During sliding the peak of the surface asperities get sheared and thereby reduces the surface roughness to some extent [237]. In unlubricated conditions the percentage reduction in CoF was more than that of lubricated conditions, as in the former the CoF solely depends on surface asperities while the latter lubricant also plays a significant role in reducing the CoF.

4.3.3.2. Worn surface analysis

Generally, in the boundary lubrication regime, wear increases with increase in temperature. The temperature under consideration is the local temperature at the contact of ball and substrate (also known as the flash temperature), which is much higher than the bulk temperature of the substrate due to frictional heating and heavy loading at the contact [5]. This flash temperature plays a significant role in the wear of ceramics. Due to high hardness and low thermal conductivity of the ceramics, the real area of contact is quite small, and the local temperature at the contact is very high [238,239]. The high flash temperature is responsible for the formation of tribofilm and phase transformation of material at the wear scar. In the reciprocating sliding condition, while using the ball as counterface, the flash temperature is higher at the center than at the edges, and preheating the substrate to a certain temperature for testing increases the datum of the flash temperature accordingly. Therefore, the increase in wear at higher temperatures can be due to the loss of viscosity of the lubricant, loss of mechanical properties of the substrate at the wear scar or combination of both. Herein, the wear obtained at 100 °C is considerably lower than wear at 30 °C. There could be many reasons for

that. Firstly, there might be a change in the properties of the lubricant at a higher temperature, which might have enhanced the wear resistance. Secondly, change in mechanical properties of the coating at the wear scar because of localised phase transformations due to high flash temperature. Thirdly, some tribo-chemical reaction might have influenced the wear surface, which would have formed a tribo-film and protected the surface from getting worn out. To investigate the above possibilities, tribotesting was done for the coated substrates without lubrication (CWL) and for uncoated substrates with lubrication (UCL) besides the coated substrates with lubrication (CL).

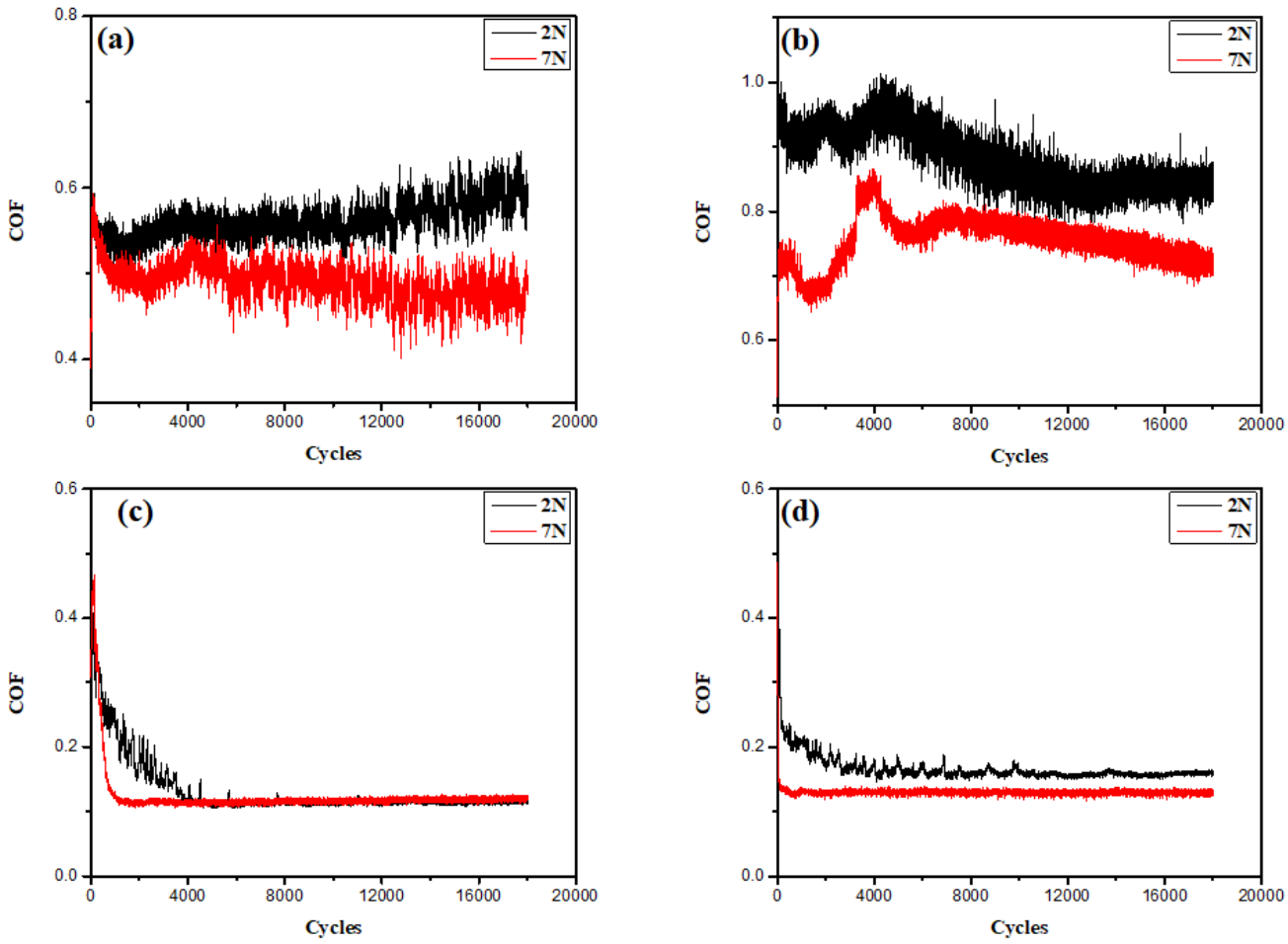

Figure. 4.6. Variation of CoF under unlubricated condition (a) at 30 °C, (b) at 100 °C; and lubricated condition (c) at 30 °C, (d) at 100 °C

Figure 4.7 shows the wear volume of multi-layered Ti/TiN coating tested under different conditions. The wear volume of CWL was higher than the wear volumes of UCL and CL, as these substrates were tribotested without any lubrication. The CL showed lower wear than UCL because of higher hardness (17 GPa) to elastic modulus ratio (240 GPa) of the coating. The wear at 7N load was higher than 2N load in all the cases because of the third body abrasion, which becomes more prominent at higher loads [240]. The CWL and UCL substrates followed the general trend of decrease in wear resistance with increase in temperature. This proves that the first two hypotheses of change in lubricant properties and change in mechanical properties of the coating with the increase in temperature are false, and the wear mechanism in the CL is being affected by some tribo-chemical interaction happening between the paraffin oil and the coating. Singer et al. [100] proposed a model of formation of tribofilm for TiN surface. A thin layer gets removed from the surface first and then gets transferred to the counterface. Since the temperature at the contact surface is very high, both the transferred layer and worn surface reacts with surrounding gases, forming respective compounds. Therefore, analysis of the worn surface was done through SEM and EDX elemental mapping.

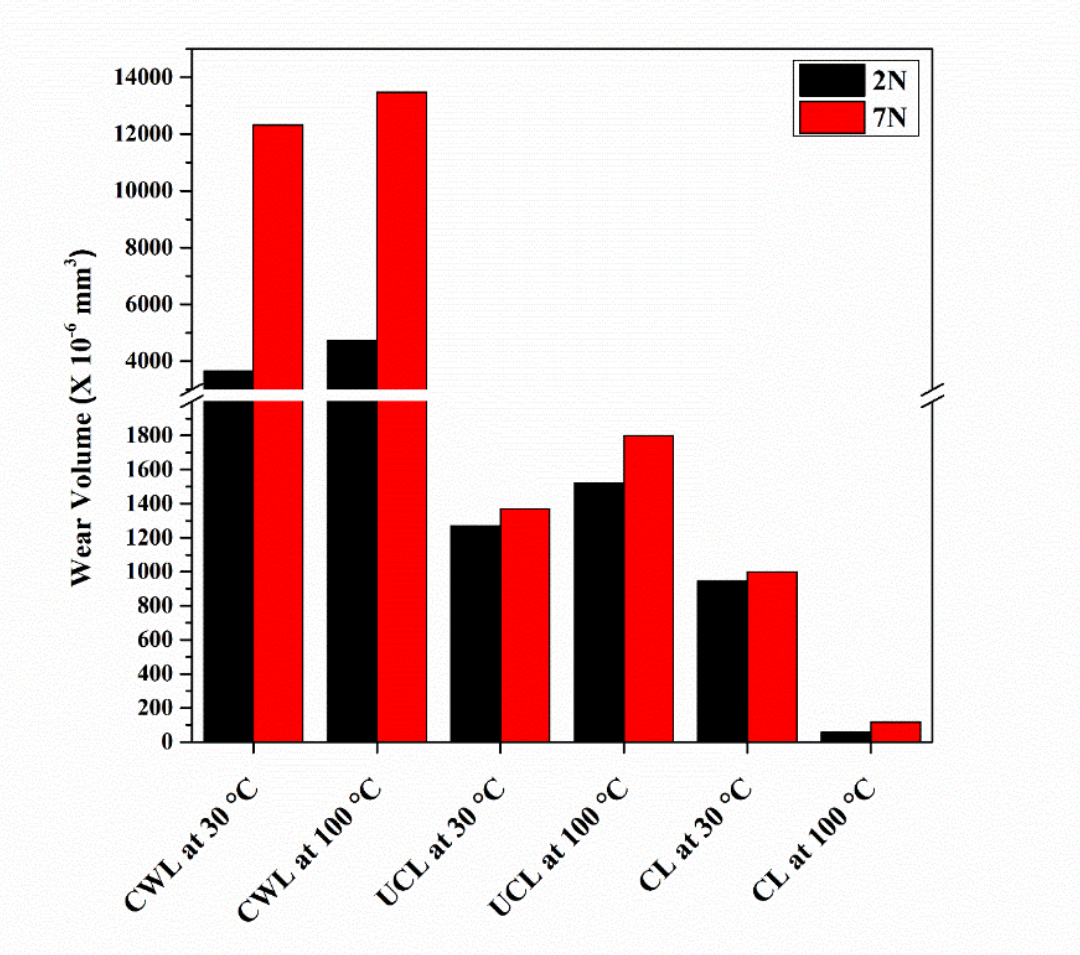

Figure. 4.7. Wear volumes under different test conditions.

4.3.3.3. SEM analysis of wear scars

Other than a little reduction in CoF at a higher load (7N), no other diversions from general behavior were observed in the results concerning the change in load. Therefore, the worn surface analysis was done for substrates tested at 7N load, which had higher wear, so that proper analysis wear mechanism could be done. **Figure** 4.8 shows SEM images and EDX elemental mapping of worn surface of CWL tested at 100 °C, the same kind of surface morphology was also seen for CWL tested at 30 °C. The surface shows signs of severe abrasive wear because of the absence of lubricant. From **Figure** 4.8a, parallel grooves, and ploughing can be seen in the direction of sliding. Micro-cracks perpendicular to the sliding direction can be seen in the

magnified image (**Figure** 4.8b); these cracks coalesce and remove a large chunk of material from the surface leading to fatigue wear. Adhesion wear depends on the metallurgical compatibility of the contacting surfaces, and the ceramic/metal surface has the least compatibility. Still, some signs of adhesion wear (very little in amount) are observed, which might be due to the interaction of the ductile metal Ti layer below the TiN layer with the steel ball. The EDX elemental mapping shows the presence of oxygen, which can be due to the formation of TiO_2 from tribo-oxidation of the Ti/TiN multi-layered coating. The formation of ceramic metal oxide on the surface also reduces the tendency of adhesive wear considerably [241].

Since the wear in CL at both the temperatures were less, the roughness profiles of the wear tracks were almost the same as that of the coated surface. The magnified SEM images show the wear mechanisms on the worn surface. **Figure** 4.9 contains the SEM and EDX elemental mapping of wear CL at both temperatures. Abrasive marks parallel to the sliding direction were observed on the worn surface at both the temperatures. Unlike CWL, the SEM images did not show the evidence of any other prominent wear mechanism. The EDX elemental mapping showed the presence of carbon and oxygen besides titanium and nitrogen. The presence of carbon is due to the use of paraffin oil, which contains long chains of carbon atoms. The presence of oxygen confirms the tribo-oxidation even in the lubricated conditions. The low wear of CL must be due to the interaction of oxide layer formed during tribotesting with the lubricant [242].

In boundary lubrication conditions, the lubricating behavior depends on the wettability of the surface in contact with the lubricant [241]. The wettability of the surface depends on its ionic character. The electronegative nature of the oxygen in TiO_2 increases the ionic behavior of Ti in the Ti/TiN multilayer coating. Therefore, the wettability of the surface increases due to the

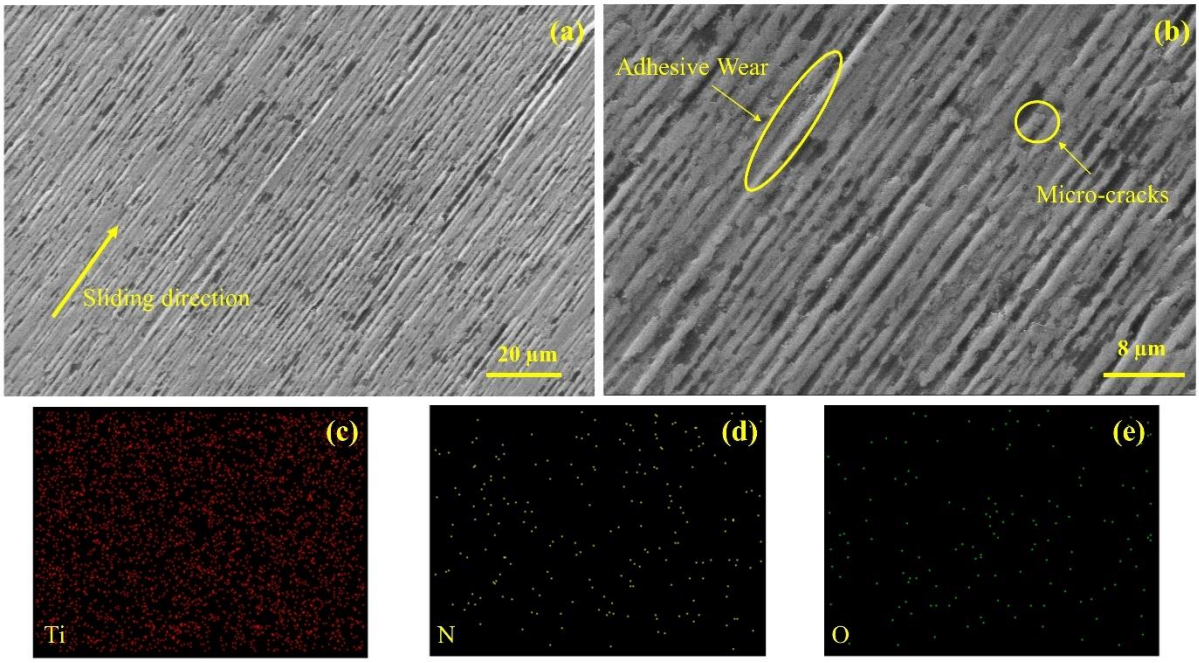

Figure. 4.8. (a) SEM image of CWL tested at 100 °C (b) magnified image of the worn surface; EDX elemental mapping of worn surface (c) Ti, (d) N and (e) O.

increase in the ionic character of the surface, and low wear is observed in the case of CL. Oxide formation was detected on both CWL (**Figure** 4.8) and CL (**Figure** 4.9), but at higher temperature huge reduction in wear in CL whereas the wear of CWL increased with increase in temperature. This can be due to the change in tribo-chemical interaction between the substrate and the ball because of the presence of paraffin oil. As the elemental mapping showed the presence of carbon, there is a possibility of forming transition metal carbides on the surface of CL, which are known for its excellent wear resistance characteristics. To get some insight into this behavior, Raman spectroscopic analysis was done for the wear scars.

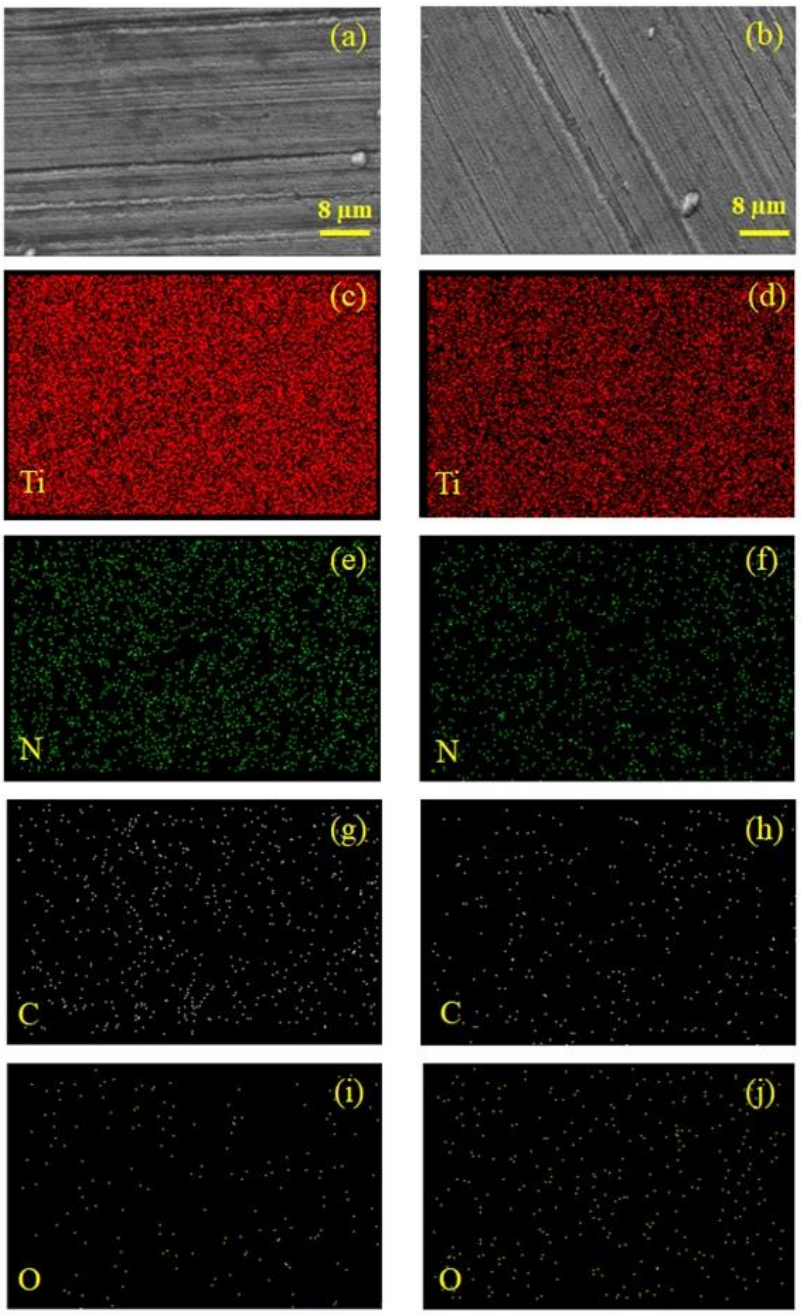

Figure. 4.9. SEM images and EDX elemental mapping of (a),(c),(e),(g),(i) CL at 30 °C; (b),(d),(f),(h),(j) CL at 100 °C.

4.3.3.4. Raman spectroscopy analysis of wear scar.

Raman spectroscopy results are shown in **Figure** 4.10 Most of the transition metal nitrides are Raman inactive because of their NaCl type of structure and atoms placed at the sites of inversion symmetry (O_h). However, the coatings deposited through magnetron sputtering contains certain impurities and vacancies (such as nitrogen and metal ions). These impurities and vacancies reduce the overall symmetry of the crystal, making the crystal Raman active by reflecting the presence of impurities and vacancies in the system. The Ti/TiN coating exhibits broad peaks in the 200-350 cm^{-1} region which are assigned to longitudinal acoustic (LA) and transverse acoustic (TA) modes, and the broad peak in the 500-600 cm^{-1} region is due to the transverse optic (TO) and longitudinal optic (LO) modes [229]. The vibrations in the acoustic and optic modes are governed by Ti and N atoms, respectively [243]. The Raman spectra of the wear scars show a shifting of peaks of the optical phonon region, which is due to the replacement of N atoms with O atoms. The Raman spectrum of CWL at 100 °C shows peaks at 221, 288, 399, and 639 cm^{-1}. The peaks in the acoustic region, i.e. 221 and 288 cm^{-1}, corresponds to the Ti atom. The presence of these Ti peaks must be due to interaction of laser with the Ti layer in the coating. Whereas, the peaks at 399 and 639 cm^{-1} corresponds to the A_{1g} and E_g modes of anatase phase of TiO_2 (denaoted as $A(A_{1g})$ and $A(E_g)$ in the **Figure** 4.10) [244]. The Raman spectrum of CWL at 30 °C showed the same peaks with lower intensities, like the ones at 100 °C, and for this reason it was not shown in **Figure** 4.10. In the Raman spectra of CL, broad peaks are present in the 200-300 cm^{-1} region corresponding to Ti atoms at both the temperatures. Broad peaks at 424 and 610 cm^{-1} are seen in CL at 30 °C and relatively sharp peaks with higher intensities at 445 and 610 cm^{-1} can be seen in CL at 100 °C. The peaks at 445 and 610 cm^{-1} correspond to the E_g and A_{1g} modes of rutile TiO_2 (denoted as $R(E_g)$ and $R(A_{1g})$ in **Figure** 4.10) [245]. The E_g peak of rutile TiO_2 in CL at 30 °C shifts to lower wavenumber at 424 cm^{-1} due to the formation of non-stoichiometric TiO_2 phase. Mazza et al.

[246] showed that the E_g peak of non-stoichiometric rutile TiO_2 shifts at a lower angle with decreasing [O]/[Ti] ratio, and the possibility of deviation reduces after thermal treatment. Therefore, when tested at 100 °C, the E_g peak is shifted back to its original position. The elemental map of oxygen on the worn surface in **Figure** 4.9 is also less pronounced at 30 °C than at 100 °C.

The peak at 424 cm^{-1} can also be confused with the non-stoichiometric peak of TiC phase [247]. As the enthalpy of formation of TiO_2 is more negative than TiC, the energy required for TiO_2 formation is less. Since no peak corresponding to TiC phase was observed at 100 °C, which means that sufficient energy for TiC formation was not reached, and the peak at 424 cm^{-1} corresponds to non- stoichiometric phase of rutile TiO_2 only.

Further analysis was done for the Raman spectrum of CL at 100 °C by deconvoluting the curve (**Figure** 4.11). Besides the peak of rutile TiO_2, i.e., 445 and 610 cm^{-1}, one additional peak was found at 547 cm^{-1} corresponding to TiN. Since the wear in CL at 100 °C was very less, the laser might have interacted with the TiN layer of the multilayer Ti/TiN coating, and the peak corresponding to the vibration of N atoms was obtained.

From the Raman results, it is clear that the tribotesting in the presence of paraffin oil led to the formation of rutile TiO_2 layer over the surface, whereas, in the absence of paraffin oil led to the formation of anatase TiO_2 layer. The rutile phase of TiO_2 is the most stable phase of TiO_2. The hardness of rutile TiO_2 is better than anatase TiO_2, and in turn, the rutile phase has a better hardness to elastic modulus ratio [248,249]. Hence the rutile phase of TiO_2 has better wear resistance property than its anatase phase. As evident from the Raman results, the rutile phase peaks become sharper and more prominent at 100 °C, indicating a higher amount of TiO_2 being formed on the surface. Therefore, the wear in CL decreases with increase in temperature due to the formation of more rutile TiO_2 on the surface. Even at 100 °C in UCL the anatase peaks

of TiO_2 were present, which means that the temperature was not high enough for anatase phase to get converted to rutile phase. However, rutile peaks can be seen in CL at 30 °C itself, which means the presence of paraffin oil favours the formation of rutile structure of TiO_2 during tribooxidation.

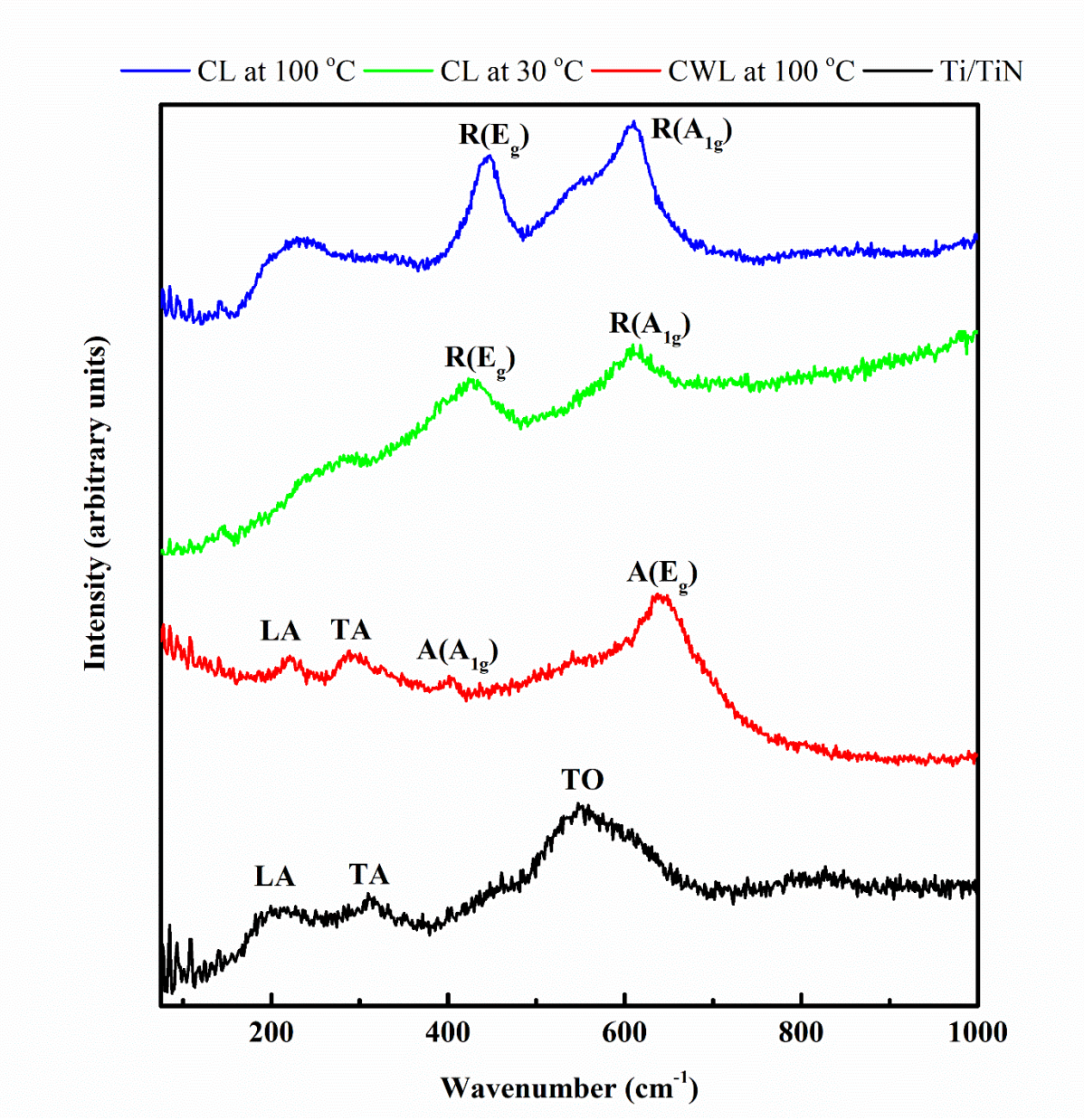

Figure. 4.10. Raman spectra of coating and worn surfaces.

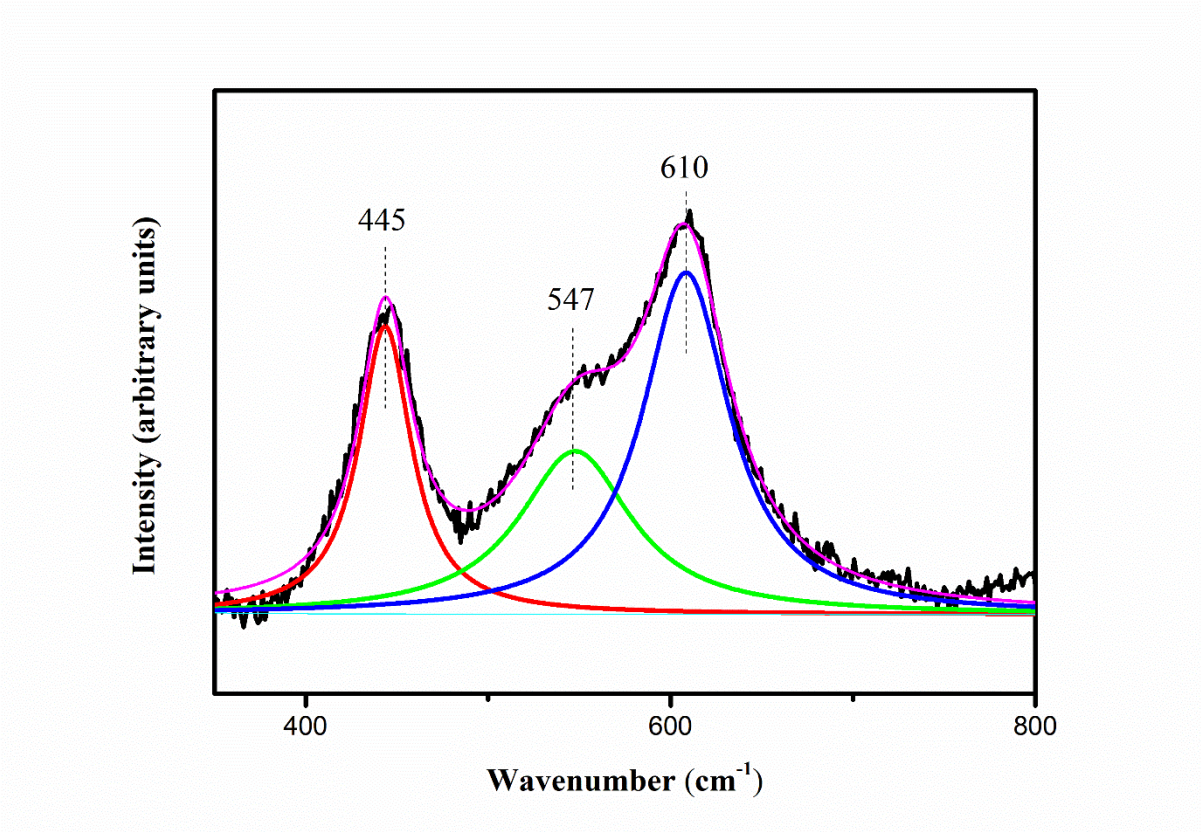

Figure. 4.11. Raman spectrum analysis of CL at 100 °C.

4.4. Summary.

Wear behavior of multi-layered Ti/TiN coatings containing SAL having low residual stress value was investigated with and without paraffin oil at different temperatures. The CoF did not change much in boundary lubrication condition. However, the CoF decreased at higher load because of shearing of surface asperities at higher load.

A significant reduction in wear was observed when tested in lubricated conditions at a higher temperature. The investigation was also done for the coated substrates without any lubricant, and for uncoated substrates under the boundary lubrication with paraffin oil. In both conditions, the wear increased with rise in temperature. These investigations proved that there is no positive influence of coating or lubricant properties in improving the wear resistance at high temperature. The worn surfaces of the coated samples in lubricated condition showed the

presence of oxygen and carbon, which showed the possibility of formation of TiO_2 or TiC on the worn surface. However, the Raman results showed the formation of TiO_2 phase, and no peaks of TiC phase were found. The unlubricated coated surface also showed the presence of TiO_2 phase, but its wear resistance decreased at higher temperature. TiO_2 exhibited different phases in lubricated and unlubricated conditions. The former had rutile phase while the latter had anatase phase. The rutile phase of TiO_2 being the most stable phase, increased the wear resistance at higher temperature. However, the chemistry behind formation of rutile phase under the influence of paraffin oil is quite complex and needs further investigation. Still one possibility can be the oxidation of thin Ti layers. Since the coating has ultrathin Ti (3.5 nm) and TiN (4 nm) layers, the possibility of oxidation of Ti layers will be way higher than TiN layers. While in dry sliding conditions the flash temperature won't be high enough to support the formation of rutile phase. But in the presence of paraffin oil there might be an increase in flash temperature due to burning of oil, as only a small drop of oil was used for tribological testing. This higher flash temperature would have supported the formation of rutile phases of TiO_2.